



University of Szeged
Institute of Informatics



Institut National de Recherche
en Informatique et en Automatique
(INRIA)

EU IMAVIS Project

Higher Order Active Contours for Tree Detection

Scientific report for the Marie Curie Fellowship program

Péter Horváth

University of Szeged, Institute of Informatics
Image Processing and Computer Graphics Department
e-mail: hp@inf.u-szeged.hu

Project Leader: Dr. Josiane Zerubia,
Projet ARIANA, Institut National de Recherche et en Automatique (INRIA), 2004 Route des
Lucioles, BP 93 FR-06902 Sophia Antipolis (France); phone: +33 4 92 38 78 65; e-mail:
Josiane.Zerubia@sophia.inria.fr

Scientific Advisor (INRIA): Dr. Ian Jermyn,
Projet ARIANA, Institut National de Recherche et en Automatique (INRIA), 2004 Route des
Lucioles, BP 93 FR-06902 Sophia Antipolis (France); phone: +33 4 92 38 76 83; e-mail:
Ian.Jermyn@sophia.inria.fr

Scientific Advisor (SZTE): Dr. Zoltan Kato,
University of Szeged, Institute of Informatics, Image Processing and Computer Graphics
Department, P.O. Box 652, H-6701 Szeged (Hungary); phone: +36 62 546 399; e-mail:
kato@inf.u-szeged.hu

Contents

1	Introduction: region modeling with active contours	3
1.1	Classical active contour energies	4
1.2	Shape descriptors	5
1.3	Higher order energies	5
1.3.1	Higher-order functionals, quadratic energies	6
2	Model for tree extraction	7
2.1	Stability analysis	7
2.2	Geometric experiments	12
2.3	Data term	12
3	Experimental results	14
3.1	Experiments on synthetic data	14
3.2	Experiments on tree images	15
4	Conclusion and future work	16
5	Acknowledgements	17
A	Stability computations	18
A.1	Length and area terms	18
A.1.1	Tangent vector	18
A.1.2	Length of the contour	18
A.1.3	Area of the contour	19
A.2	Quadratic energy	19
B	Other approaches for tree extraction	25

1 Introduction: region modeling with active contours

The primary goal of any segmentation algorithm is to divide the input image into disjoint parts such that they belong to distinct objects in the scene. The solution of this problem is usually based on the low-level features (*e.g.* color, texture, motion, etc.) of the surface patches. Purely data driven methods however cannot deal very well with high noise, cluttered background or occlusions. Hence the idea of incorporating some prior knowledge about the shape of the objects has been considered by many researchers. Early approaches for shape prior were quite generic, enforcing some kind of homogeneity and contour smoothness [4, 7, 11, 16, 23, 24]. For example, [16, 24] uses a Markovian smoothness prior (basically a Potts model [3]); [4, 16] uses a line process to control the formation of region boundaries; and active contour models [23] have been using elasticity, rigidity, contour length, balloon or area minimizing forces [7, 11] in order to favor smooth closed curves. In spite of their simplicity, these methods proved to be very efficient in dealing with noisy images.

There have been a great deal of work on statistical shape modeling [20]. These methods are relying on a kind of template matching: The object under investigation is of known shape (template) and its allowed deformations are learned a priori [30, 31]. This knowledge is then summarized in a statistical model which is incorporated into a variational [9, 14, 38] or probabilistic [21, 32] model. These models often borrow ideas from mathematical pattern theory developed by Grenander [19]: The basic assumption is that the deformations are a result of some kind of transformations (usually affine) applied to the reference shape. The modeling step involves the estimation and representation of the underlying transformations and the prior will penalize strong deviations. Such models are useful when we have a clear idea how the objects look like and the segmentation is driven by recognizing the object in the image data. A typical application is medical image processing where well known objects (*e.g.* organs) has to be segmented. For example, in [9] a variational method with shape priors using an atlas has been proposed. The priors were restricted to a parametric deformation between the reference shape and the active contour.

For many applications, however, the assumption of a parametric deformation is too restrictive or impractical to use. An interesting approach is presented in [37] where basic geometrical constraints are modeled by quadratic energy functionals in a level set framework. The method is applied to road extraction from satellite images using a prior which favors network-like objects.

In this report we further develop the method in [37] for modeling a ‘gas of circles’. For that purpose, we used a new generation of active contours, called **Higher Order Active Contours** (HOACs). HOACs are able to capture higher order interactions between the contour points providing a great possibility to integrate prior shape information into the model with translation and rotation invariance. Furthermore, they can handle more than one objects during the segmentation.

There is a broad range of applications where such a segmentation model can be used *e.g.* in remote sensing (craters, trees, missile silos, etc.), and in medical or biological imaging (cells, organisms, etc.). Herein, we apply the method to the extraction of tree crowns from aerial images provided by the French National Forest Inventory (INF). We have concentrated our efforts on making different statistics from the segmentation *e.g.* the density of trees in a given area (trees/ha), the mean diameter of the crowns etc. From the extracted data the forestry can control its efficiency and can plan its work. In Fig. 1, we show an example with different planted forests, where one can use our method.

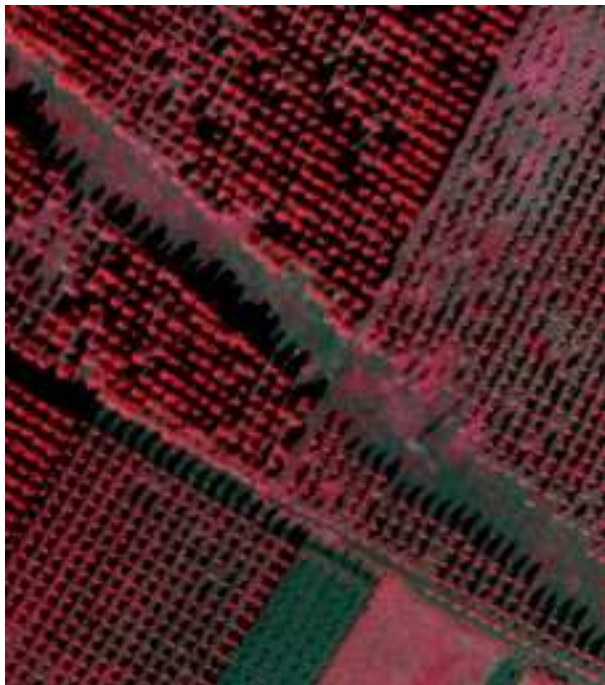


Figure 1: Real image with planted forest ©IFN.

In the rest of this section, we present classical active contour models and extensions allowing the incorporation of shape information, and then describe and define HOACs and quadratic active contour energies. In section 2, we describe the proposed HOAC model for tree extraction. The stability of the geometric term is then analyzed, which places constraints on the parameter values we can use. We present experimental results with the geometric term. A data term based on the image intensity and gradient is introduced. In section 3, we present results on synthetic data as well as on aerial images.

1.1 Classical active contour energies

Active contours were introduced in 1988 by Kass *et al.* [23]. Snakes or active contours are curves defined within an image domain that can move under the influence of internal forces coming from within the curve itself and an external force computed from the image data. The internal and external forces are defined so that the snake will conform to an object boundary or other desired features within an image. In 1991 Cohen published the ‘Balloon model’ [11]. This model gives an extra term, the area term, which yields a constant pressure. With the aid of this pressure we are able to remove the contour from the local minima caused by the small gradients. ‘Geodesic’ active contours [6, 7, 25, 29] removed the parameterization dependency of the early models. To accomplish this we use the length of the boundary as an energy term in a non-Euclidean metric on Ω determined by the image. The above presented energies are integrals of functions over the contour. Chan and Vese introduced an active contour method without using edges. They try to divide the image plane into a foreground and a background based on image intensity [8]. Paragios *et al.* [35] and Jehan-Besson *et al.* [22] introduced methods based on the integrals of functions over the interior.

In the above active contour models, the prior and likelihood terms are algebraic combinations of integrals over the region or the contour. With these models we can only represent

local interactions between contour points, where local means constructed from the derivatives of the curve at each point. The dependency on derivatives means that interactions take place within fixed size neighbourhoods. In addition, because the degree of the derivatives involved is typically small, the neighbourhoods are small.

This limitation makes the expressive power of the prior term weak. If we just observe the first derivatives, then the two possible Euclidean invariant properties are the length and the area.

1.2 Shape descriptors

To eliminate some limitations of the prior term, various approaches have been proposed to integrate information into the model. Most of the models use shape matching to match the segmented image to a given image or set of images. Shape matching is a complex and well studied part of image processing. We can find an overview of the published approaches in [41]. Leventon *et al.* represent the shape as a signed distance function. They use a Gaussian distribution on the principal components of variation around the mean distance function acquired from training data as a shape prior [28]. Cremers *et al.* [12] extended the Mumford-Shah functional [33] with statistical shape prior information. They represent a contour as a spline, and learn a Gaussian distribution from the control points of the spline. The statistical prior restricts the contour deformations to the subspace of learnt deformations. In 2002 Cremers *et al.* introduced statistical shape prior information with diffusion snakes [14]. In 2003 Cremers and Soatto introduced a method based on pseudo-distance between the shapes [13]. Chen *et al.* defined an energy based on gradient and the mean shape of the observed object [10]. The prior shape term evaluates the similarity of the shape of the contour to that of the reference shape through the computation of the distance function using the Fast Marching method of Sethian [39]. Foulonneau *et al.* introduced a method based on Legendre moments for region-based active contours [15], using the Euclidean invariance property of the shape moments. They combined their method with the Chan and Vese model [8].

The above presented methods have some common properties. Given one or more training examples or a mean object, they try to locate a simple object on the image plane. The evolution of the contour tries to find the given object or the best matching from the given set of objects. These methods are useful in some cases but they have their limitations. They do not work if not only one but **many objects** are present on the image plane, or if the regions to be extracted **cannot be defined as small variations around a mean shape**.

1.3 Higher order energies

In this section we present a general higher order active contour model introduced by Rochery *et al.* [37]. We also present quadratic energies, which are a special case of higher order active contours, and we present an example of a possible interaction function. As we wrote above, classical active contour energies are constructed from single integrals over the contour. In contrast HOACs include multiple integrals over the contour. They are able to represent higher order interactions between the contour points. Here we introduce some notations which we will use later. Let Ω be a bounded subset of \mathbb{R}^2 and $I : \Omega \rightarrow \mathbb{R}$ be an image. The contour Γ is defined as a **1-chains** $\Gamma : S^1 \rightarrow \Omega$ and $\tau(p) = \Gamma'(p)$ is the tangent vector to Γ at p .

1.3.1 Higher-order functionals, quadratic energies

HOACs are constructed from multiple integrals over the contour. The general form of such integrals is the following: given an n -form F on Ω^n , we pull it back to the domain of $\Gamma^{\otimes n}$ and integrate it:

$$E(\Gamma) = \int_{(\partial R)^n} F = \int_{(dom\Gamma)^n} (\Gamma^{\otimes n})^* F. \quad (1)$$

From now we will focus on quadratic energies ($n = 2$). We can rewrite the energy function as:

$$\begin{aligned} E(\Gamma) &= \int_{(\partial R)^2} F \\ &= \int_{(dom\Gamma)^2} (\Gamma \otimes \Gamma)^* F \\ &= \int \int \tau(p) \cdot F(\Gamma(p), \Gamma(p')) \cdot \tau(p') dp dp', \end{aligned} \quad (2)$$

where $F(x, x')$, for each $(x, x') \in \Omega^2$, is a matrix. The operator F allows us to **model non-trivial interactions** between different contour points.

Using this term, Rochery *et al.* defined the following higher order active contour model, imposing the Euclidian invariance of the prior term:

$$E_G(\Gamma) = \lambda_C L(\Gamma) + \alpha_C A(\Gamma) - \frac{\beta_C}{2} \int \int \tau(t) \cdot \tau(t') \Phi(R(t, t')) dt dt', \quad (3)$$

where L is the length of the boundary, A is the area of its interior and $R(t, t') = |\Gamma(t) - \Gamma(t')|$ is the distance between $\Gamma(t)$ and $\Gamma(t')$. They introduced the following interaction function Φ :

$$\Phi(x) = \begin{cases} 1 & \text{if } x < d_{\min} - \epsilon, \\ 0 & \text{if } x > d_{\min} + \epsilon, \\ \frac{1}{2} \left(1 - \frac{x - d_{\min}}{\epsilon} - \frac{1}{\pi} \sin\left(\pi \frac{x - d_{\min}}{\epsilon}\right) \right) & \text{otherwise.} \end{cases} \quad (4)$$

In our experiments we used this interaction function, but we note that we could use other monotonic decreasing functions (e.g. exponential, Bessel).

2 Model for tree extraction

In this section, we will define our model for tree extraction. It has two parts: a model of the region occupied by trees in the image domain, for which we will use E_G ; and a model of the appearance of the trees in the image. The latter will be described in subsection 2.3. In the first two subsections, we concentrate on E_G . We want to adjust the parameters in the model so that configurations consisting of collections of circles of approximately a certain radius r_0 are stable (or nearly stable). In order for this to work, the circles themselves should be stable. Stability means that if the shape of a circle of radius r_0 is changed slightly, it will relax back into the circle. We thus need to choose parameters so that a circle of radius r_0 is a minimum of E_G . To do so, we start from a circle of radius r_0 , and expand the energy in a Taylor series to second order around this contour. We will then adjust the parameters so that the first derivative is zero, which tells us that the circle is an energy extremum, and so that the second derivative is positive definite, which tells us that the extremum is a minimum. This calculation is described in subsection 2.1. In subsection 2.2, we present experiments with the energy E_G showing empirically that the calculation does indeed work.

2.1 Stability analysis

Since we are expanding E_G around a circle, it is easiest to express the contour in terms of polar coordinates r, θ on Ω . A circle of radius r_0 centred on the origin is then given by $\Gamma_0(t) = (r_0(t), \theta_0(t))$, where:

$$\begin{aligned} r_0(t) &= r_0 \\ \theta_0(t) &= t \end{aligned}$$

and $t \in [0, 2\pi)$ is the curve parameter. We are interested in the behaviour of small variations $\delta\Gamma = (\delta r, \delta\theta)$ around this contour, that is in calculating $E_G(\Gamma_0 + \delta\Gamma)$ as a power series in $\delta\Gamma$. The first thing to notice is that tangential changes in Γ do not affect the energy, since it is parametrization invariant. We can therefore set $\delta\theta = 0$, and concentrate on δr .

It turns out to be easiest to perform the calculation by expressing δr in terms of the Fourier basis for the tangent space at Γ_0 . Thus $\Gamma = \Gamma_0 + \delta\Gamma$ can be written as:

$$\begin{aligned} r(t) &= r_0 + \delta r(t) = r_0 + \sum_k a_k e^{ir_0 kt} \\ \theta(t) &= \theta_0(t) \end{aligned} \tag{5}$$

For further computations we need the derivatives of $r(t)$ and $\theta(t)$ with respect to t , which are given by:

$$\begin{aligned} \dot{r}(t) &= \delta \dot{r}(t) = \sum_k a_k i r_0 k e^{ir_0 kt} \\ \dot{\theta}(t) &= 1. \end{aligned}$$

To express the length and area terms we need the tangent vector τ over t which we can write as follows:

$$\tau(t) = \dot{r}(t) \frac{\partial}{\partial r} + \dot{\theta}(t) \frac{\partial}{\partial \theta},$$

and the absolute value of this tangent vector to second order (for more details see Appendix A.1.1):

$$|\tau(t)| = r_0 \left\{ 1 + \sum_k \frac{a_k}{r_0} e^{ir_0 kt} + \frac{1}{2} \sum_{kk'} a_k a_{k'}^+ k k' e^{ir_0(k-k')t} \right\}.$$

where + indicates complex conjugation. Now we are able to express the **length** and the **area** of the contour for a given r_0 to second order as follows:

$$L(\Gamma) = \int_0^{2\pi} |\tau(t)| dt = 2\pi r_0 \left\{ 1 + \frac{a_0}{r_0} + \frac{1}{2} \sum_k |a_k|^2 k^2 \right\} \quad (6)$$

$$A(\Gamma) = \int_0^{2\pi} \int_0^{r(\theta)} r dr d\theta = \pi r_0^2 + 2\pi r_0 a_0 + \pi \sum_k |a_k|^2. \quad (7)$$

To determine the expression of the **quadratic term** we need the dot product of the tangent vectors at t and t' as well as the distance between those two points. The dot product can be written as:

$$\begin{aligned} \tau(t) \cdot \tau(t') &= \cos(\theta' - \theta) \cdot [r_0^2 + r_0 \delta r' + r_0 \delta r + \delta r \delta r' + \delta \dot{r} \delta \dot{r}'] + \\ &\quad \sin(\theta' - \theta) \cdot [r_0 \delta \dot{r}' - r_0 \delta \dot{r} - \delta \dot{r} \delta r' + \delta r \delta \dot{r}'], \end{aligned}$$

where $r = r(t)$ and $\theta = \theta(t)$. For more details see Appendix A.2. We can express the distance between two points on the contour to second order, ordered by δr and $\delta r'$, as:

$$\begin{aligned} |\Gamma(t') - \Gamma(t)| &= 2r_0 \sin \left| \frac{\Delta\theta}{2} \right| + \delta r \sin \left| \frac{\Delta\theta}{2} \right| + \delta r' \sin \left| \frac{\Delta\theta}{2} \right| + \\ &\quad \delta r^2 \frac{1}{4r_0} A(\Delta\theta) + \delta r'^2 \frac{1}{4r_0} A(\Delta\theta) - \delta r \delta r' \frac{1}{2r_0} A(\Delta\theta), \end{aligned}$$

where $\Delta\theta = \theta' - \theta$, $\Delta t = t' - t$ and $A(\Delta t) = \left(\frac{\cos^2(\frac{\Delta\theta}{2})}{\sin|\frac{\Delta\theta}{2}|} \right)$. Now we approximate $\Phi(|\Gamma(t') - \Gamma(t)|)$ by the following rule: $f(X) = f(X_0) + f'(X_0)(X_1 + X_2) + \frac{1}{2} f''(X_0) X_1^2$, where X_0, X_1 and X_2 are the constant, first and second order terms in X . We use the notation $X_0 = 2r_0 \sin \left| \frac{\Delta\theta}{2} \right|$

$$\begin{aligned} \Phi(|\Gamma(t') - \Gamma(t)|) &= \Phi(X_0) + \delta r \sin \left| \frac{\Delta\theta}{2} \right| \Phi'(X_0) + \delta r' \sin \left| \frac{\Delta\theta}{2} \right| \Phi'(X_0) \\ &\quad + \delta r^2 \left[\frac{1}{4r_0} A(\Delta\theta) \cdot \Phi'(X_0) + \frac{1}{2} \sin^2 \frac{\Delta\theta}{2} \cdot \Phi''(X_0) \right] \\ &\quad + \delta r'^2 \left[\frac{1}{4r_0} A(\Delta\theta) \cdot \Phi'(X_0) + \frac{1}{2} \sin^2 \frac{\Delta\theta}{2} \cdot \Phi''(X_0) \right] \\ &\quad + \delta r \delta r' \left[-\frac{1}{2r_0} A(\Delta\theta) \cdot \Phi'(X_0) + \sin^2 \frac{\Delta\theta}{2} \cdot \Phi''(X_0) \right]. \end{aligned}$$

Now let $G(t', t) = \tau(t') \cdot \tau(t)\Phi(|\Gamma(t') - \Gamma(t)|)$. Then we have:

$$\begin{aligned}
G(t', t) = & \underbrace{r_0^2 \cos \Delta\theta \Phi(X_0)}_{F_{00,even}} \\
& + \delta r \cdot r_0 \cos \Delta\theta \left\{ \Phi(X_0) + r_0 \sin \left| \frac{\Delta\theta}{2} \right| \Phi'(X_0) \right\} \\
& + \underbrace{\delta r' \cdot r_0 \cos \Delta\theta \left\{ \Phi(X_0) + r_0 \sin \left| \frac{\Delta\theta}{2} \right| \Phi'(X_0) \right\}}_{F_{10,even}} \\
& - \delta \dot{r} \cdot r_0 \sin \Delta\theta \Phi(X_0) \\
& + \underbrace{\delta \dot{r}' \cdot r_0 \sin \Delta\theta \Phi(X_0)}_{F_{11,odd}} \\
& + \delta r^2 \cdot r_0 \cos \Delta\theta \left\{ \frac{1}{4} A(\Delta\theta) \Phi'(X_0) + \frac{1}{2} r_0 \sin^2 \frac{\Delta\theta}{2} \Phi''(X_0) + \sin \left| \frac{\Delta\theta}{2} \right| \Phi'(X_0) \right\} \\
& + \underbrace{\delta r'^2 \cdot r_0 \cos \Delta\theta \left\{ \frac{1}{4} A(\Delta\theta) \Phi'(X_0) + \frac{1}{2} r_0 \sin^2 \frac{\Delta\theta}{2} \Phi''(X_0) + \sin \left| \frac{\Delta\theta}{2} \right| \Phi'(X_0) \right\}}_{F_{20,even}} \\
& + \underbrace{\delta r \delta r' \cdot \cos \Delta\theta \left\{ \Phi(X_0) + 2r_0 \sin \left| \frac{\Delta\theta}{2} \right| \Phi'(X_0) - \frac{1}{2} r_0 A(\Delta\theta) \Phi'(X_0) + r_0^2 \sin^2 \frac{\Delta\theta}{2} \Phi''(X_0) \right\}}_{F_{21,even}} \\
& - \underbrace{\delta r \delta \dot{r} \cdot r_0 \sin \left| \frac{\Delta\theta}{2} \right| \sin \Delta\theta \Phi'(X_0)}_{F_{22,odd}} \\
& + \delta r \delta r' \cdot \sin \Delta\theta \left\{ \Phi(X_0) + r_0 \sin \left| \frac{\Delta\theta}{2} \right| \Phi'(X_0) \right\} \\
& - \underbrace{\delta r' \delta \dot{r} \cdot \sin \Delta\theta \left\{ \Phi(X_0) + r_0 \sin \left| \frac{\Delta\theta}{2} \right| \Phi'(X_0) \right\}}_{F_{23,odd}} \\
& + \delta r' \delta \dot{r}' \cdot r_0 \sin \left| \frac{\Delta\theta}{2} \right| \sin \Delta\theta \Phi'(X_0) \\
& + \underbrace{\delta \dot{r} \delta \dot{r}' \cdot \cos \Delta\theta \Phi(X_0)}_{F_{24,even}}.
\end{aligned}$$

For simplicity we introduced the notation $F_{00}..F_{24}$ for the terms in G . Now we can express

the quadratic term as:

$$\begin{aligned}
\int \int_0^{2\pi} G(t', t) dt' dt &= \int \int_0^{2\pi} F_{00} dt' dt + \int \int_0^{2\pi} (\delta r + \delta r') F_{10} dt' dt \\
&+ \int \int_0^{2\pi} (\delta \dot{r}' - \delta \dot{r}) F_{11} dt' dt + \int \int_0^{2\pi} (\delta r^2 + \delta r'^2) F_{20} dt' dt \\
&+ \int \int_0^{2\pi} \delta r \delta r' F_{21} dt' dt + \int \int_0^{2\pi} (\delta r' \delta \dot{r}' - \delta r \delta \dot{r}) F_{22} dt' dt \\
&+ \int \int_0^{2\pi} (\delta r \delta \dot{r}' - \delta r' \delta \dot{r}) F_{23} dt' dt + \int \int_0^{2\pi} \delta \dot{r} \delta \dot{r}' F_{24} dt' dt.
\end{aligned}$$

Substituting the decomposition of δr into its Fourier components from equation (5), we find (for more details see Appendix A.2):

$$\begin{aligned}
\int \int_0^{2\pi} G(t', t) dt' dt &= 2\pi \int_0^{2\pi} F_{00} dp + a_0 4\pi \int_0^{2\pi} F_{10} dp \\
&+ \sum_k |a_k|^2 2\pi \left\{ \left[2 \int_0^{2\pi} F_{20} dp + \int_0^{2\pi} F_{21} e^{ir_0 kp} dp \right] \right. \\
&\left. + k \left[2ir_0 \int_0^{2\pi} F_{23} e^{ir_0 kp} dp \right] + k^2 \left[r_0^2 \int_0^{2\pi} F_{24} e^{ir_0 kp} dp \right] \right\}. \quad (8)
\end{aligned}$$

Using equations (6), (7) and (8), we can now express the energy function (3) up to the second order, as:

$$\begin{aligned}
E_G(\Gamma) = E(\Gamma_0 + \delta\Gamma) &= \left[\lambda_C 2\pi r_0 + \alpha_C \pi r_0^2 - \frac{\beta_C}{2} 2\pi \int_0^{2\pi} F_{00} dp \right] \\
&+ a_0 \left[\lambda_C 2\pi + \alpha_C 2\pi r_0 - \frac{\beta_C}{2} 4\pi \int_0^{2\pi} F_{10} dp \right] \\
&+ \sum_k |a_k|^2 \left(\lambda_C \pi r_0 k^2 + \alpha_C \pi \right. \\
&\left. - \frac{\beta_C}{2} 2\pi \left\{ \left[2 \int_0^{2\pi} F_{20} dp + \int_0^{2\pi} F_{21} e^{ir_0 kp} dp \right] \right. \right. \\
&\left. \left. + k \left[2ir_0 \int_0^{2\pi} F_{23} e^{ir_0 kp} dp \right] + k^2 \left[r_0^2 \int_0^{2\pi} F_{24} e^{ir_0 kp} dp \right] \right\} \right). \quad (9)
\end{aligned}$$

Now we present a setting of the parameters where the curve is a stable circle by a given radius r_0 . During our experiments we used the interaction function (4) introduced by Rochery *et al.* [37]. Our goal is to set the parameter values so that the energy is minimized by a circle of radius r_0 , stable for all the frequencies. Thus we set the parameters so that the second term of the energy function becomes 0 when the radius r is equal to r_0 and the third term becomes positive for every value of k (the Fourier frequencies). In this case the instabilities for all of k -s increase the contour's energy. If we equate the second term to zero we can write the parameter β_C as a function of α_C , λ_C and r_0 :

$$\beta_c(\lambda_c, \alpha_c, r_0) = \frac{\lambda_c + \alpha_c r_0}{\int_0^{2\pi} F_{10} dp}. \quad (10)$$

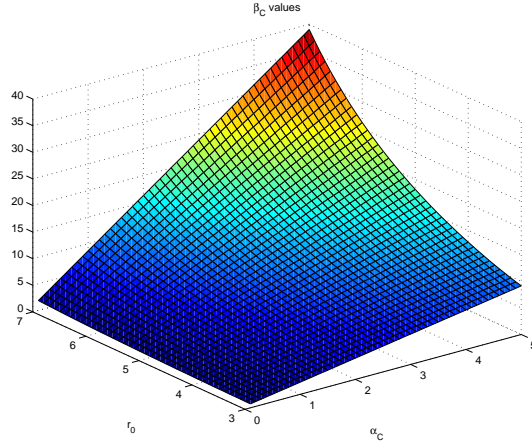


Figure 2: The values of β_C for a given λ_C , α_C and r_0 ($\lambda_C = 1.0$, $\alpha_C = 0.0 - 5.0$ and $r_0 = 3.0 - 7.0$).

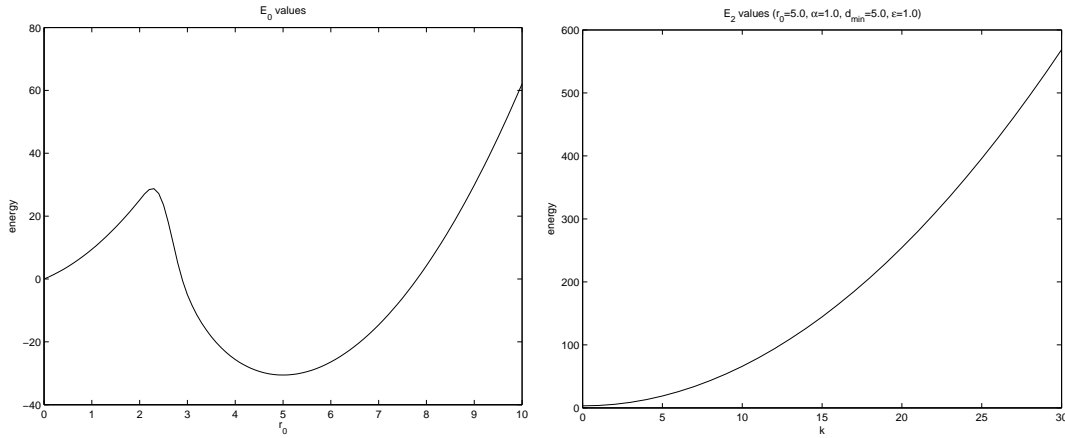


Figure 3: Left: The energy plot of E_0 versus r for a given $\alpha = 1.0$, $\beta = 1.036$ and $r_0 = 5.0$. It can be seen that the function has a local minima at r_0 and has a local maxima between 0 and r_0 . Right: Energy plot of E_2 versus k , it is apparent that the energy is positive over all frequencies.

Fig. 2 shows the values of β_C for various α_C and r_0 settings. With the aid of the 0th, 1st and 2nd order terms of the energy function we can present the value of the energy for various parameter settings. The zeroth order term (*i.e.* the energy of a circle of radius r_0) is defined as:

$$E_0(r_0, \alpha_c, \beta_c) = \lambda_C 2\pi r_0 + \alpha_C \pi r_0^2 - \frac{\beta_C}{2} 2\pi \int_0^{2\pi} F_{00} dp, \quad (11)$$

since we try to stabilize the radius of the circle at r_0 , the energy must have a minimum at r_0 . Fig. 3 (left handside) shows the energy plot of E_0 . As you can see the minimum of the energy is located at r_0 . The first order energy term is:

$$E_1(r_0, \alpha_c, \beta_c) = \lambda_C 2\pi + \alpha_C 2\pi r_0 - \frac{\beta_C}{2} 4\pi \int_0^{2\pi} F_{10} dp. \quad (12)$$

This energy is 0 over the whole domain, because we computed β_C from the equation $E_1 = 0$.

The second order energy term can be computed as:

$$E_2(r_0, \alpha_c, \beta_c, k) = \lambda_C \pi r_0 k^2 + \alpha_C \pi - \frac{\beta_C}{2} 2\pi \left\{ \left[2 \int_0^{2\pi} F_{20} dp + \int_0^{2\pi} F_{21} e^{ir_0 k p} dp \right] + k \left[2ir_0 \int_0^{2\pi} F_{23} e^{ir_0 k p} dp \right] + k^2 \left[r_0^2 \int_0^{2\pi} F_{24} e^{ir_0 k p} dp \right] \right\}. \quad (13)$$

With the aid of E_2 we can choose parameters for which E_2 is positive for all the values of the k . In Fig. 3 (right handside) we can see one possible configuration for a given r_0 . The energy over k is always non-negative, which means the contour is stable for every possible frequency. In the example of Fig. 3 we choose a radius ($r_0 = 5.0$), and we calculate the possible β_C values for a given set of α_C . Afterwards we substitute the computed α_C and β_C values in the function (13), and we check where E_2 remains positive for every value of k . In our example we can produce stable circles with the following parameters: $r_0 = 5.0$; $\alpha_C = 1.0$; $\beta_C \cong 1.036$; $\lambda_C = 1.0$; $d_{min} = 5.0$; $\epsilon = 1.0$.

2.2 Geometric experiments

The experimental results with the geometric term are shown in Fig. 4. In the first column we find the initial curve(s). We used three different parameter settings for different radii ($r_0 = 15.0, 10.0, 5.0$), the results of the evolution can be seen in the second, third and fourth columns. In the first experiment (first line) the initial shape was a circle of radius 32 pixels. After the evolution, the stable state, which can be seen in the 2nd-4th columns, is a circle with the desired radius in every case. In the second line we see an interesting phenomenon. Some of the initial curves vanish. In the second column just two circles survive of the original 8 and in the third just 4. The explanation for this is interesting. The energy function over the radius has a minimum at r_0 and it is 0 if the radius is 0. Between r_0 and 0 there is a point where the energy has a local maximum. If the initial radius is less than this local maximum then the shape vanishes. In the fourth column all the shapes survive the evolution.

In the third experiment, the initial shapes were four rectangles. For all the radii, all the circles are in the expected places and have the correct size. In the last experiment, the initial shapes were four different objects. With the first two radii, the final shapes of the evolution are four circles of the appropriate size, but with the smallest radius the final shapes are more than four circles. This is due to the area term, since the shape and size of the curve is far from the desired circle. The area term is stronger and begins to extract the skeleton. Later, the quadratic energy becomes stronger and creates the circles.

2.3 Data term

In real applications our model has two terms. The geometric part which provides the circular shape of the segmented parts, and the data term that guarantees that the circles are in suitable locations. The energy we use is:

$$E(\Gamma) = E_G(\Gamma) + \epsilon_C \int \hat{\mathbf{n}}(p) \cdot \nabla I(p) dp + \delta_C^{in} \int_{\Omega_{in}} \frac{(I(p) - \mu_{in})^2}{2\sigma_{in}^2} dp + \delta_C^{out} \int_{\Omega_{out}} \frac{(I(p) - \mu_{out})^2}{2\sigma_{out}^2} dp, \quad (14)$$

where $E_G(\Gamma)$ is the geometric energy. The second term ensures that the contour stops at large image gradients. We could ask ourselves why is this term not enough; the answer is that we

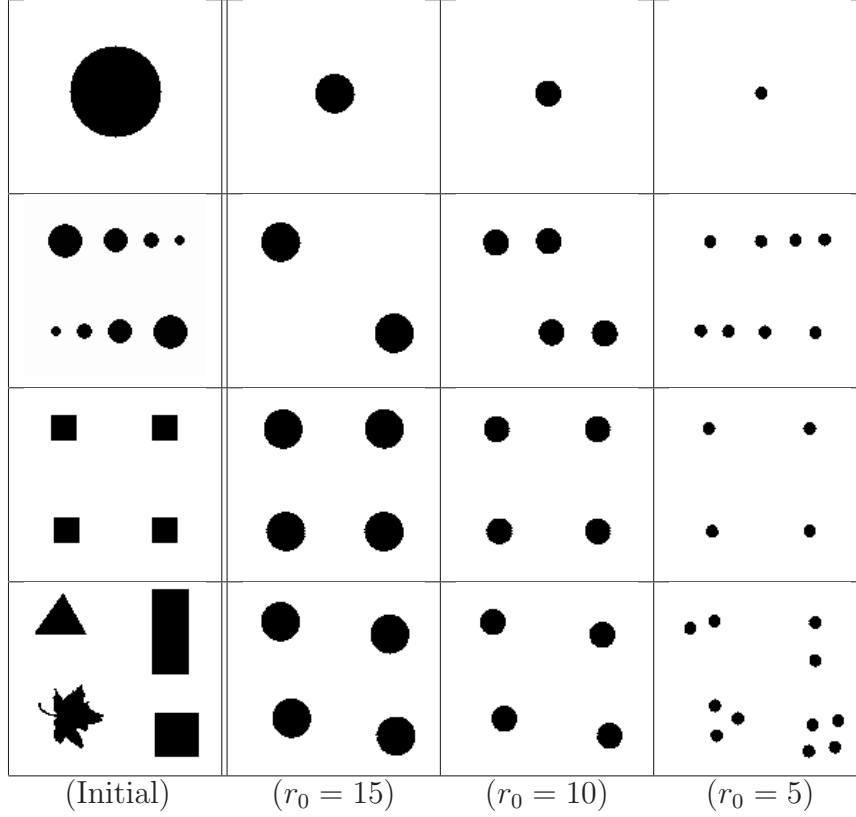


Figure 4: Experimental results using the geometric term: the first column shows the initial shapes; the other columns show the stable states for various choices of the radius.

can get incorrect circles when the gradient is 0 or close to 0. For this reason we introduced an additional energy term which is based on the Mahalanobis distance between the intensity of the image and the mean and the variance of the inside and outside regions (μ_{in} , μ_{out} , σ_{in} and σ_{out}). The parameters ϵ_C , δ_C^{in} and δ_C^{out} control the segmentation. The energy is minimized by a gradient descent and the descent equation is:

$$\hat{\mathbf{n}} \cdot \frac{\partial \Gamma}{\partial t} = -\kappa - \alpha_C - \epsilon_C \nabla^2 I + \delta_C^{in} \frac{(I - \mu_{in})^2}{2\sigma_{in}^2} - \delta_C^{out} \frac{(I - \mu_{out})^2}{2\sigma_{out}^2} + 2\beta_C \int (\hat{\mathbf{R}}(p, p') \cdot \hat{\mathbf{n}}(p')) \Psi'(R(p, p')) dp', \quad (15)$$

where $\hat{\mathbf{R}}(p, p') = \frac{\Gamma(p) - \Gamma(p')}{|\Gamma(p) - \Gamma(p')|}$, κ is the curvature over the contour and α_C is the parameter of the area term in equation (3). To evolve the contour we use a level-set framework introduced by Osher and Sethian [34].

3 Experimental results

In this section we present our results on synthetic and real data. For a brief overview of tree extraction and remotely sensed images see Appendix B.

3.1 Experiments on synthetic data

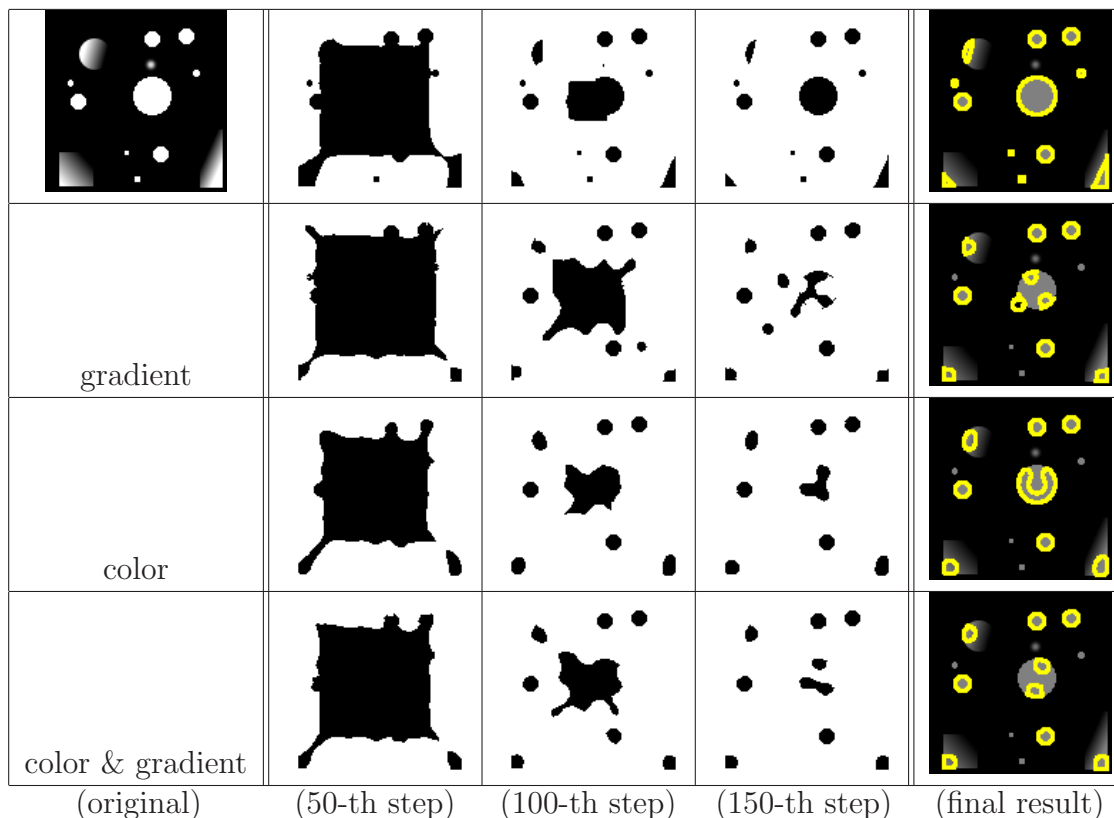


Figure 5: Experiments on synthetic data

Our experimental results can be seen in Fig. 5. The original image (left upper corner) has objects with variable shape and size along with sharp and smooth edges. We want to eliminate the objects that are different from circles or that have a too small radius. We also want to partially detect areas with larger dimensions. The 2^{nd} - 4^{th} columns represent the contour evolution after 50, 100 and 150 iterations. In the last column we present the final segmentation.

The result obtained without the quadratic term can be seen in the first row where all the objects were detected using suitable parameter settings. In the second row can be seen the result with the quadratic term, in the formulation only the image gradient is used as the data term. The circles with desired radius were detected and the smaller shapes were eliminated. By the big smooth circle the circle was detected by the darkest part because the gradient values are the biggest here. Similarly by the smoothed rectangles the detected circles are also on the lightest part. In the case of the biggest circle we found two smaller circles inside the object and one outside. This is because the gradient is big over the boundary of this circle, and the circles inside push out the third circle. The results using the intensity term can be seen in the third row. The too small object was also eliminated. By the smoothed object the detected

circles are also by the lightest part because the color intensity is here the biggest. In the case of a biggest circle the contour grew as an arm. In the last row we can see the results obtained by combining the gradient and the intensity term. All the desired objects were successfully detected, in the big circle we found two separated circles. The intensity term yields that the circle has to be inside, the gradient determines that it has to be on the boundary and the prior results in the circular shape.

3.2 Experiments on tree images

Here we present our first results on real images. We tested our model on an aerial image of resolution 54 cm/pixel provided by the IFN. The image shows poplar stands located in Saône et Loire (France).

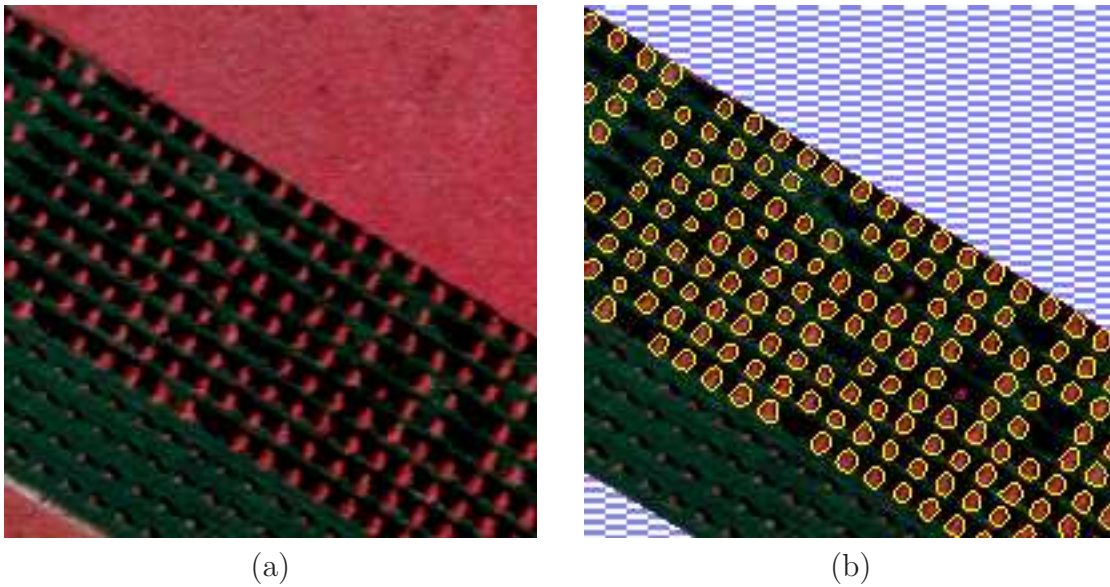


Figure 6: Real image with a planted forest (a) and the segmentation result (b) ©IFN.

In Fig. 6 one can see a regularly planted poplar forest. In the upper part of the image the trees are older with bigger crowns (8-10 pixels \approx 4-5 m), while in the lower part there are younger trees; we set the desired r_0 to detect the former but not the latter trees. In Fig. 6, we are using the proposed algorithm only in the central part of the image. We do not deal with the dashed areas.

In Fig. 7 can be seen a small piece of a slightly irregularly planted poplar forest. The image is difficult, because the intensities of the crowns are very varied, some trees overlap, and the gradients are very smooth. For that reason classical methods (such as classical AC; thresholding; edge detectors) do not work on this image.

In the table can be seen some statistics computed from the results. In the second row is the number of detected trees, in the third row the area of planted trees in the image, and in the last row the density of trees in a hectare.

Figure#	6	7
Trees#:	152	53
Area (ha):	0.63	0.48
Average (trees/ha):	241.2	112.7

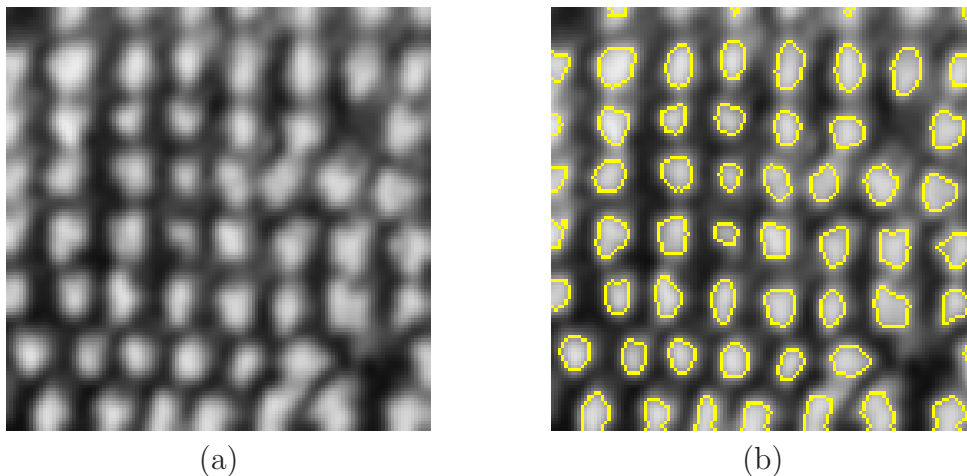


Figure 7: Planted forest (a) and the segmentation result (b) ©IFN.

4 Conclusion and future work

We have introduced new parameter settings for higher order active contours to produce circles with desired radius. With active contour methods published earlier it is not possible to model higher order interactions between the contour points. This technique enable us to model these interactions.

Several models were presented for tree detection (see Appendix B). Some of the models use line or edge detection, in this case shape prior cannot be introduced. Methods, using template matching can introduce low-level shape information, but they use intensity-based segmentation. Our method uses intensity as well as edge information, which results in a better segmentation.

In Fig. 6 we concentrated on the part of the image located out of the dashed areas because we were not able to eliminate continuous light areas (e.g. fields, houses, roads...), and we also could not handle textures. We will introduce a new data term to solve these problems.



Figure 8: Internal vs. external interactions (a), joint circles (b).

In our future work we will concentrate on various problems that have arisen. In Fig. 8(a) can be seen two circles with the same radii. If the distance between the circles is equal to the given diameter then the interaction between the points p and p' is exactly the same as the interaction between the points q and q' . This creates undesirable interactions between circles. We will develop a new energy function to eliminate this problem.

Our main goal is to count the trees and create statistics from the segmentation (e.g. trees/km², mean diameter of the crowns...). We will try two different methods for counting. It is well known that the integral of the curvature over a closed curve is 2π , so that we can

express the number of the circles N as:

$$N = \frac{\int_{\Gamma} ds\kappa}{2\pi}$$

The other approach is to determine the shock graph of the segmentation [40]. The number of 4th order shocks gives the number of trees, in this way we will be able to handle the case where the trees are overlapping, as illustrated in Fig. 8(b). We can also compute the distance transformation while we compute the shock graph, and thus compute radii: the radius of the circle is just the distance value at the 4th order shocks.

Finally, we will investigate the possibility of automatic parameter estimation.

5 Acknowledgements

This work was carried out during a six month stay by Péter Horváth in the Ariana research group at INRIA Sophia Antipolis, supported by the IMAVIS EU project (FP5 IHP-MCHT99) and partially supported by the Balaton PAI. A one-week visit to INRIA by Dr. Zoltan Kato was supported by the Balaton PAI. The authors would like to thank the French National Forest Inventory (IFN) for the forest images.

A Stability computations

A.1 Length and area terms

In this section we present the polar coordinate forms of the **length** and **area** terms, and their expression in terms of the Fourier coefficients of the deviation from Γ_0 .

A.1.1 Tangent vector

We defined $r(t)$, $\theta(t)$ and $\tau(t)$ in section 2.1, now we compute the length of the tangent vector using the fact that the squared distance with polar coordinates is $ds^2 = dr^2 + r^2 d\theta$. We can express $|\tau(t)|^2$ as:

$$\begin{aligned} |\tau(t)|^2 &= [\dot{r}(t)]^2 + [r(t)\dot{\theta}(t)]^2 \\ &= \sum_{k,k'} [a_k i r_0 k e^{i r_0 k t}] [a_{k'}^+ - i r_0 k' e^{i r_0 k' t}] + \\ &\quad r_0^2 + 2 r_0 \sum_k a_k e^{i r_0 k t} + \sum_{k,k'} a_k a_{k'}^+ e^{i r_0 (k-k') t} (1 + r_0^2 k k'). \end{aligned}$$

From this expression we can denote the length of the tangent vector $|\tau(t)|$, using the approximation form $\sqrt{1+x} \approx 1 + \frac{1}{2}x - \frac{1}{8}x^2$:

$$\begin{aligned} |\tau(t)| = \sqrt{|\tau(t)|^2} &= r_0 \left\{ 1 + 2 \sum_k \frac{a_k}{r_0} e^{i r_0 k t} + \sum_{k,k'} a_k a_{k'}^+ e^{i r_0 (k-k') t} \left(\frac{1}{r_0^2} k k' \right) \right\} \\ &= r_0 \left\{ 1 + \sum_k \frac{a_k}{r_0} e^{i r_0 k t} + \frac{1}{2} \sum_{k,k'} a_k a_{k'}^+ e^{i r_0 (k-k') t} \left(\frac{1}{r_0^2} k k' \right) - \right. \\ &\quad \left. \frac{1}{8} \sum_{k,k'} \frac{a_k a_{k'}^+}{r_0 r_0} e^{i r_0 (k-k') t} + \dots \right\} \\ &= r_0 \left\{ 1 + \sum_k \frac{a_k}{r_0} e^{i r_0 k t} + \frac{1}{2} \sum_{kk'} a_k a_{k'}^+ k k' e^{i r_0 (k-k') t} \right\}. \end{aligned} \tag{16}$$

A.1.2 Length of the contour

Since we can express the length term as the integral of the tangent vector over the curve, we can express the length in terms of the Fourier coefficients as:

$$\begin{aligned} L(\Gamma) = \int_0^{2\pi} |\tau(t)| dt &= r_0 \left\{ 2\pi + 2\pi \frac{a_0}{r_0} + \pi \sum_k |a_k|^2 k^2 \right\} \\ &= 2\pi r_0 \left\{ 1 + \frac{a_0}{r_0} + \frac{1}{2} \sum_k |a_k|^2 k^2 \right\}. \end{aligned} \tag{17}$$

A.1.3 Area of the contour

We can write the area of the contour as the integral of the radius, and in terms of the Fourier coefficients as:

$$\begin{aligned}
A(\Gamma) &= \int_0^{2\pi} \int_0^{r(\theta)} r dr d\theta = \int_0^{2\pi} \frac{1}{2} r^2(\theta) d\theta \\
&= \frac{1}{2} \int_0^{2\pi} \left(r_0^2 + 2r_0 \sum_k a_k e^{ir_0 k \theta} + \sum_{k,k'} a_k a_{k'}^+ e^{ir_0(k-k')\theta} \right) d\theta \\
&= \frac{1}{2} \left(2\pi r_0^2 + 4\pi r_0 a_0 + 2\pi \sum_k |a_k|^2 \right) \\
&= \pi r_0^2 + 2\pi r_0 a_0 + \pi \sum_k |a_k|^2.
\end{aligned}$$

A.2 Quadratic energy

In this section, we introduce the expression of the quadratic term in terms of the Fourier coefficients of the deviation from Γ_0 . First we recall the quadratic energy term:

$$E_Q(\Gamma) = -\frac{\beta_C}{2} \int \int \tau(t') \tau(t) \Phi(|\Gamma(t') - \Gamma(t)|) dt dt', \quad (18)$$

To compute the tangential dot product we express the tangent vectors with polar coordinates. Using the well known definition: $\tau(t) = [\dot{x}(t), \dot{y}(t)]$ and $\tau(t') = [\dot{x}(t'), \dot{y}(t')]$, we can write the dot product as $\tau(t) \cdot \tau(t') = \dot{x}(t) \cdot \dot{x}(t') + \dot{y}(t) \cdot \dot{y}(t')$. We can express $x(t)$ and $y(t)$ with the polar coordinates as:

$$\begin{aligned}
x(t) &= [r_0 + \delta r(t)] \cos(\theta(t)) = r_0 \cos(\theta(t)) + \delta r(t) \cos(\theta(t)), \\
y(t) &= [r_0 + \delta r(t)] \sin(\theta(t)) = r_0 \sin(\theta(t)) + \delta r(t) \sin(\theta(t)),
\end{aligned}$$

and the derivatives of the coordinates with the polar coordinates:

$$\begin{aligned}
\dot{x}(t) &= -r_0 \sin(\theta(t)) \dot{\theta}(t) + \delta \dot{r} \cos(\theta(t)) - \delta r \sin(\theta(t)) \dot{\theta}(t), \\
\dot{y}(t) &= r_0 \cos(\theta(t)) \dot{\theta}(t) + \delta \dot{r} \sin(\theta(t)) + \delta r \cos(\theta(t)) \dot{\theta}(t).
\end{aligned}$$

Now we introduce for simplicity the following notations: $x = x(t)$, $y = y(t)$, $\dot{x} = \dot{x}(t)$, $\dot{y} = \dot{y}(t)$, $s(x) = \sin(x)$, $c(x) = \cos(x)$, $r = r(t)$, $\theta = \theta(t)$ and $\Delta\theta = \theta' - \theta$. Now we write the dot product as:

$$\begin{aligned}
\dot{x} \cdot \dot{x}' &= r_0^2 s(\theta) s(\theta') - r_0 \delta \dot{r}' s(\theta) c(\theta') + r_0 \delta r' s(\theta) s(\theta') \\
&\quad - r_0 \delta \dot{r} s(\theta') c(\theta) + \delta \dot{r} \delta r' c(\theta) c(\theta') - \delta \dot{r} \delta r' s(\theta') c(\theta) \\
&\quad + r_0 \delta r s(\theta) s(\theta') - \delta r \delta \dot{r}' s(\theta) c(\theta') + \delta r \delta r' s(\theta) s(\theta'), \\
\dot{y} \cdot \dot{y}' &= r_0^2 c(\theta) c(\theta') + r_0 \delta \dot{r}' s(\theta') c(\theta) + r_0 \delta r' c(\theta) c(\theta') \\
&\quad + r_0 \delta \dot{r} s(\theta) c(\theta') + \delta \dot{r} \delta r' s(\theta) s(\theta') + \delta \dot{r} \delta r' s(\theta) c(\theta') \\
&\quad + r_0 \delta r c(\theta) c(\theta') + \delta r \delta \dot{r}' s(\theta') c(\theta) + \delta r \delta r' c(\theta) c(\theta').
\end{aligned}$$

$$\begin{aligned}
\dot{x} \cdot \dot{x}' + \dot{y} \cdot \dot{y}' &= [s(\theta)s(\theta') + c(\theta)c(\theta')] \cdot [r_0^2 + r_0\delta r' + r_0\delta r + \delta r\delta r' + \delta\dot{r}\delta\dot{r}'] + \\
&\quad [s(\theta')c(\theta) - s(\theta)c(\theta')] \cdot [r_0\delta\dot{r}' - r_0\delta\dot{r} - \delta\dot{r}\delta r' + \delta r\delta\dot{r}'] \\
&= c(\theta' - \theta) \cdot [r_0^2 + r_0\delta r' + r_0\delta r + \delta r\delta r' + \delta\dot{r}\delta\dot{r}'] + \\
&\quad s(\theta' - \theta) \cdot [r_0\delta\dot{r}' - r_0\delta\dot{r} - \delta\dot{r}\delta r' + \delta r\delta\dot{r}'].
\end{aligned} \tag{19}$$

We can express the square distance between $\Gamma(t')$ and $\Gamma(t)$ as:

$$\begin{aligned}
|\Gamma(t') - \Gamma(t)|^2 &= [(x(t') - x(t))^2 + (y(t') - y(t))^2] \\
&= [(r_0 + \delta r') \cdot c(\theta') - (r_0 + \delta r) \cdot c(\theta)]^2 \\
&\quad + [(r_0 + \delta r') \cdot s(\theta') - (r_0 + \delta r) \cdot s(\theta)]^2 \\
&= r_0^2 c^2(\theta') + \delta r'^2 c^2(\theta') + r_0^2 c^2(\theta) + \delta r^2 c^2(\theta) \\
&\quad + 2r_0\delta r' c^2(\theta') - 2r_0^2 c(\theta)c(\theta') - 2r_0\delta r c(\theta)c(\theta') \\
&\quad - 2r_0\delta r' c(\theta)c(\theta') - 2\delta r'\delta r c(\theta)c(\theta') + 2r_0\delta r c^2(\theta) \\
&\quad + r_0^2 s^2(\theta') + \delta r'^2 s^2(\theta') + r_0^2 s^2(\theta) + \delta r^2 s^2(\theta) \\
&\quad + 2r_0\delta r' s^2(\theta') - 2r_0^2 s(\theta)s(\theta') - 2r_0\delta r s(\theta)s(\theta') \\
&\quad - 2r_0\delta r' s(\theta)s(\theta') - 2\delta r'\delta r s(\theta)s(\theta') + 2r_0\delta r s^2(\theta) \\
&= 2r_0^2(1 - c(\Delta\theta)) + \delta r(2r_0 - 2r_0c(\Delta\theta)) + \delta r'(2r_0 - 2r_0c(\Delta\theta)) \\
&\quad + \delta r^2 + \delta r'^2 - 2c(\Delta\theta)\delta r\delta r' \\
&= 2r_0^2(1 - c(\Delta\theta)) + 2r_0(1 - c(\Delta\theta))(\delta r + \delta r') \\
&\quad + \delta r^2 + \delta r'^2 - 2c(\Delta\theta)\delta r\delta r' \\
&= 2r_0^2(1 - c(\Delta\theta)) \left\{ 1 + \frac{1}{r_0}(\delta r + \delta r') + \frac{\delta r^2 + \delta r'^2 - 2c(\Delta\theta)\delta r\delta r'}{2r_0^2(1 - c(\Delta\theta))} \right\}.
\end{aligned}$$

With the $\sqrt{1+x} \approx 1 + \frac{1}{2}x - \frac{1}{8}x^2$ approximation we can determine $|\Gamma(t') - \Gamma(t)|$ up to the second order:

$$\begin{aligned}
|\Gamma(t') - \Gamma(t)| &= 2r_0 \sin \left| \frac{\Delta\theta}{2} \right| \left\{ 1 + \frac{1}{2r_0}(\delta r + \delta r') + \right. \\
&\quad \left. \underbrace{\frac{\delta r^2 + \delta r'^2 - 2\cos(\Delta\theta)\delta r\delta r'}{4r_0^2(1 - \cos(\Delta\theta))} - \frac{(\delta r + \delta r')^2}{8r_0^2}}_* \right\},
\end{aligned}$$

where the * term can be written as:

$$\begin{aligned}
* &= \frac{2\delta r^2 + 2\delta r'^2 - 4\cos(\Delta\theta)\delta r\delta r'}{8r_0^2(1 - \cos(\Delta\theta))} - \frac{(\delta r^2 + 2\delta r\delta r' + \delta r'^2)(1 - \cos(\Delta\theta))}{8r_0^2(1 - \cos(\Delta\theta))} \\
&= \frac{(\delta r^2 - 2\delta r\delta r' + \delta r'^2)}{8r_0^2} \left(\frac{1 + \cos(\Delta\theta)}{1 - \cos(\Delta\theta)} \right) \\
&= \frac{(\delta r^2 - 2\delta r\delta r' + \delta r'^2)}{8r_0^2} \left(\frac{\cos^2\left(\frac{\Delta\theta}{2}\right)}{\sin\left|\frac{\Delta\theta}{2}\right|} \right).
\end{aligned}$$

Let $A(\Delta\theta) = \left(\frac{\cos^2\left(\frac{\Delta\theta}{2}\right)}{\sin\left|\frac{\Delta\theta}{2}\right|} \right)$. Then the distance between $\Gamma(t')$ and $\Gamma(t)$ to second order:

$$\begin{aligned}
|\Gamma(t') - \Gamma(t)| &= 2r_0 \sin \left| \frac{\Delta\theta}{2} \right| + \delta r \sin \left| \frac{\Delta\theta}{2} \right| + \delta r' \sin \left| \frac{\Delta\theta}{2} \right| + \\
&\quad \delta r^2 \frac{1}{4r_0} A(\Delta\theta) + \delta r'^2 \frac{1}{4r_0} A(\Delta\theta) - \delta r\delta r' \frac{1}{2r_0} A(\Delta\theta).
\end{aligned} \tag{20}$$

Here we present the approximation of $\Phi(|\Gamma(t') - \Gamma(t)|)$ as $\Phi(X) = \Phi(X_0) + \Phi'(X_0)(X_1 + X_2) + \frac{1}{2}\Phi''(X_0)X_1^2$, where X_0, X_1 and X_2 are the constant, first and second order terms respectively. Using the notation $X_0 = 2r_0 \sin \left| \frac{\Delta\theta}{2} \right|$, we have:

$$\begin{aligned}
\Phi(|\Gamma(t') - \Gamma(t)|) &= \Phi(X_0) + \delta r \sin \left| \frac{\Delta\theta}{2} \right| \Phi'(X_0) + \delta r' \sin \left| \frac{\Delta\theta}{2} \right| \Phi'(X_0) \\
&\quad + \delta r^2 \left[\frac{1}{4r_0} A(\Delta\theta) \cdot \Phi'(X_0) + \frac{1}{2} \sin^2 \frac{\Delta\theta}{2} \cdot \Phi''(X_0) \right] \\
&\quad + \delta r'^2 \left[\frac{1}{4r_0} A(\Delta\theta) \cdot \Phi'(X_0) + \frac{1}{2} \sin^2 \frac{\Delta\theta}{2} \cdot \Phi''(X_0) \right] \\
&\quad + \delta r \delta r' \left[-\frac{1}{2r_0} A(\Delta\theta) \cdot \Phi'(X_0) + \sin^2 \frac{\Delta\theta}{2} \cdot \Phi''(X_0) \right]. \quad (21)
\end{aligned}$$

We write $G(t', t) = \tau(t') \cdot \tau(t) \Phi(|\Gamma(t') - \Gamma(t)|)$, we have:

$$\begin{aligned}
G(t', t) &= \\
&\underbrace{r_0^2 \cos \Delta\theta \Phi(X_0)}_{F_{00,even}} \\
&+ \delta r \cdot r_0 \cos \Delta\theta \left\{ \Phi(X_0) + r_0 \sin \left| \frac{\Delta\theta}{2} \right| \Phi'(X_0) \right\} \\
&+ \delta r' \cdot r_0 \cos \Delta\theta \left\{ \Phi(X_0) + r_0 \sin \left| \frac{\Delta\theta}{2} \right| \Phi'(X_0) \right\} \\
&\quad \underbrace{\hspace{10em}}_{F_{10,even}} \\
&- \delta \dot{r} \cdot r_0 \sin \Delta\theta \Phi(X_0) \\
&+ \delta \dot{r}' \cdot r_0 \sin \Delta\theta \Phi(X_0) \\
&\quad \underbrace{\hspace{10em}}_{F_{11,odd}} \\
&+ \delta r^2 \cdot r_0 \cos \Delta\theta \left\{ \frac{1}{4} A(\Delta\theta) \Phi'(X_0) + \frac{1}{2} r_0 \sin^2 \frac{\Delta\theta}{2} \Phi''(X_0) + \sin \left| \frac{\Delta\theta}{2} \right| \Phi'(X_0) \right\} \\
&+ \delta r'^2 \cdot r_0 \cos \Delta\theta \left\{ \frac{1}{4} A(\Delta\theta) \Phi'(X_0) + \frac{1}{2} r_0 \sin^2 \frac{\Delta\theta}{2} \Phi''(X_0) + \sin \left| \frac{\Delta\theta}{2} \right| \Phi'(X_0) \right\} \\
&\quad \underbrace{\hspace{10em}}_{F_{20,even}} \\
&+ \delta r \delta r' \cdot \cos \Delta\theta \left\{ \Phi(X_0) + 2r_0 \sin \left| \frac{\Delta\theta}{2} \right| \Phi'(X_0) - \frac{1}{2} r_0 A(\Delta\theta) \Phi'(X_0) + r_0^2 \sin^2 \frac{\Delta\theta}{2} \Phi''(X_0) \right\} \\
&\quad \underbrace{\hspace{10em}}_{F_{21,even}} \\
&- \delta r \delta \dot{r} \cdot r_0 \sin \left| \frac{\Delta\theta}{2} \right| \sin \Delta\theta \Phi'(X_0) \\
&\quad \underbrace{\hspace{10em}}_{F_{22,odd}} \\
&+ \delta r \delta \dot{r}' \cdot \sin \Delta\theta \left\{ \Phi(X_0) + r_0 \sin \left| \frac{\Delta\theta}{2} \right| \Phi'(X_0) \right\} \\
&- \delta r' \delta \dot{r} \cdot \sin \Delta\theta \left\{ \Phi(X_0) + r_0 \sin \left| \frac{\Delta\theta}{2} \right| \Phi'(X_0) \right\} + \\
&\quad \underbrace{\hspace{10em}}_{F_{23,odd}}
\end{aligned}$$

$$\begin{aligned}
& +\delta r' \delta \dot{r}' \cdot r_0 \sin \left| \frac{\Delta \theta}{2} \right| \sin \Delta \theta \Phi'(X_0) \\
& +\delta \dot{r} \delta \dot{r}' \cdot \underbrace{\cos \Delta \theta \Phi(X_0)}_{F_{24, \text{even}}}. \tag{22}
\end{aligned}$$

For simplicity we use the notations $F_{00}..F_{24}$. We can express the quadratic energy $\int \int_0^{2\pi} G(t', t) dt' dt$ as:

$$\begin{aligned}
\int \int_0^{2\pi} G(t', t) dt' dt &= \int \int_0^{2\pi} F_{00} dt' dt + \int \int_0^{2\pi} (\delta r + \delta r') F_{10} dt' dt + \\
& \int \int_0^{2\pi} (\delta \dot{r}' - \delta \dot{r}) F_{11} dt' dt + \int \int_0^{2\pi} (\delta r^2 + \delta r'^2) F_{20} dt' dt + \\
& \int \int_0^{2\pi} \delta r \delta r' F_{21} dt' dt + \int \int_0^{2\pi} (\delta r' \delta \dot{r}' - \delta r \delta \dot{r}) F_{22} dt' dt + \\
& \int \int_0^{2\pi} (\delta r \delta \dot{r}' - \delta r' \delta \dot{r}) F_{23} dt' dt + \int \int_0^{2\pi} \delta \dot{r} \delta \dot{r}' F_{24} dt' dt. \tag{23}
\end{aligned}$$

Substituting $\delta r(t) = \sum_k a_k e^{i r_0 k t}$ and $\delta \dot{r}(t) = \sum_k a_k i r_0 k e^{i r_0 k t}$, and denoting $p = t - t'$, we have the following expressions for the various terms:

- $\int \int F_{00} dt dt'$

$$\int \int_0^{2\pi} f(r_0, t - t') dt dt' = 2\pi \int f(r_0, p) dp$$

- $\int \int \delta r F_{10} dt dt' = \int \int \delta r' F_{10} dt dt'$:

$$\begin{aligned}
\int \int_0^{2\pi} \delta r f(r_0, t - t') dt dt' &= \int \int \sum_k a_k e^{i r_0 k t} f(r_0, t - t') dt dt' \\
&= \sum_k a_k \int \int e^{i r_0 k (p+t')} f(r_0, p) dp dt' \\
&= \sum_k a_k \int e^{i r_0 k t'} dt' \int e^{i r_0 k p} f(r_0, p) dp \\
&= \sum_k a_k 2\pi \delta(k) \int e^{i r_0 k p} f(r_0, p) dp \\
&= 2\pi a_0 \int f(r_0, p) dp
\end{aligned}$$

- $\int \int \delta \dot{r} F_{11} dt dt' = - \int \int \delta \dot{r}' F_{11} dt dt'$:

$$\begin{aligned}
\int \int_0^{2\pi} \delta \dot{r} f(r_0, t - t') dt dt' &= \int \int \sum_k a_k k i r_0 e^{i r_0 k t} f(r_0, t - t') dt dt' \\
&= \sum_k a_k k i r_0 \int \int e^{i r_0 k (p+t')} f(r_0, p) dp dt' \\
&= \sum_k a_k k i r_0 \int e^{i r_0 k t'} dt' \int e^{i r_0 k p} f(r_0, p) dp \\
&= \sum_k a_k k i r_0 2\pi \delta(k) \int e^{i r_0 k p} f(r_0, p) dp \\
&= 0
\end{aligned}$$

- $\int \int \delta r^2 F_{20} dt dt' = \int \int \delta r'^2 F_{20} dt dt'$:

$$\begin{aligned}
\int \int_0^{2\pi} \delta r^2 f(r_0, t - t') dt dt' &= \int \int \sum_k \sum_{k'} a_k a_{k'} e^{i r_0 (k+k') t} f(r_0, t - t') dt dt' \\
&= \sum_k \sum_{k'} a_k a_{k'} \int \int e^{i r_0 (k+k') (p+t')} f(r_0, p) dp dt' \\
&= \sum_k \sum_{k'} a_k a_{k'} \int e^{i r_0 (k+k') t'} dt' \int e^{i r_0 (k+k') p} f(r_0, p) dp \\
&= \sum_k \sum_{k'} a_k a_{k'} 2\pi \delta(k + k') \int e^{i r_0 (k+k') p} f(r_0, p) dp \\
&= \sum_k a_{+k} a_{-k} 2\pi \int f(r_0, p) dp \\
&= 2\pi \sum_k |a_k|^2 \int f(r_0, p) dp.
\end{aligned}$$

- $\int \int F_{21} dt dt'$:

$$\begin{aligned}
\int \int_0^{2\pi} \delta r \delta r' f(r_0, t - t') dt dt' &= \int \int \sum_k \sum_{k'} a_k a_{k'} e^{i r_0 (k t + t' k')} f(r_0, t - t') dt dt' \\
&= \sum_k \sum_{k'} a_k a_{k'} \int \int e^{i r_0 k (p+t')} e^{i r_0 k' t'} f(r_0, p) dp dt' \\
&= \sum_k \sum_{k'} a_k a_{k'} \int e^{i r_0 (k+k') t'} dt' \int e^{i r_0 k p} f(r_0, p) dp \\
&= \sum_k \sum_{k'} a_k a_{k'} 2\pi \delta(k + k') \int e^{i r_0 k p} f(r_0, p) dp \\
&= \sum_k a_{+k} a_{-k} 2\pi \int e^{i r_0 k p} f(r_0, p) dp \\
&= 2\pi \sum_k |a_k|^2 \int e^{i r_0 k p} f(r_0, p) dp.
\end{aligned}$$

- $\int \int \delta r' \delta \dot{r}' F_{22} dt dt' = - \int \int \delta r \delta \dot{r} F_{22} dt dt' :$

$$\begin{aligned}
\int \int_0^{2\pi} \delta r \delta \dot{r} f(r_0, t - t') dt dt' &= \int \int \sum_k \sum_{k'} a_k a_{k'} i r_0 k e^{i r_0 (k+k') t} f(r_0, t - t') dt dt' \\
&= \sum_k \sum_{k'} a_k a_{k'} i r_0 k \int \int e^{i r_0 (k+k') (p+t')} f(r_0, t - t') dt dt' \\
&= \sum_k \sum_{k'} a_k a_{k'} i r_0 k \int e^{i r_0 (k+k') t'} dt' \int e^{i r_0 (k+k') p} f(r_0, p) dp \\
&= \sum_k \sum_{k'} a_k a_{k'} i r_0 k 2\pi \delta(k + k') \int e^{i r_0 (k+k') p} f(r_0, p) dp \\
&= 0.
\end{aligned}$$

- $\int \int \delta r \delta \dot{r}' F_{23} dt dt' = - \int \int \delta r' \delta \dot{r} F_{23} dt dt' :$

$$\begin{aligned}
\int \int_0^{2\pi} \delta r' \delta \dot{r} f(r_0, t - t') dt dt' &= \int \int \sum_k \sum_{k'} a_k a_{k'} i r_0 k' e^{i r_0 (k t' + k' t)} f(r_0, t - t') dt dt' \\
&= \sum_k \sum_{k'} a_k a_{k'} i r_0 k' \int \int e^{i r_0 (k' p + k' t' + k t')} f(r_0, t - t') dp dt' \\
&= \sum_k \sum_{k'} a_k a_{k'} i r_0 k' \int e^{i r_0 (k+k') t'} dt' \int e^{i r_0 k' p} f(r_0, p) dp \\
&= \sum_k \sum_{k'} a_k a_{k'} i r_0 k 2\pi \delta(k + k') \int e^{i r_0 (k+k') p} f(r_0, p) dp \\
&= \sum_k 2\pi |a_k|^2 i r_0 k \int e^{i r_0 k p} f(r_0, p) dp
\end{aligned}$$

- $\int \int F_{24} dt dt' :$

$$\begin{aligned}
\int \int_0^{2\pi} \delta \dot{r} \delta \dot{r}' f(r_0, t - t') dt dt' &= \int \int \sum_k \sum_{k'} a_k a_{k'} i^2 r_0^2 k k' e^{i r_0 (k t + k' t')} f(r_0, t - t') dt dt' \\
&= \sum_k \sum_{k'} a_k a_{k'} (-1) r_0^2 k k' \int \int e^{i r_0 (k(p+t') + k' t')} f(r_0, p) dp dt' \\
&= \sum_k \sum_{k'} a_k a_{k'} (-1) r_0^2 k k' \int e^{i r_0 t' (k+k')} dt' \int e^{i r_0 k p} f(r_0, p) dp \\
&= \sum_k \sum_{k'} a_k a_{k'} (-1) r_0^2 k k' 2\pi \delta(k + k') \int e^{i r_0 k p} f(r_0, p) dp \\
&= \sum_k 2\pi |a_k|^2 r_0^2 k^2 \int e^{i r_0 k p} f(r_0, p) dp.
\end{aligned}$$

We can express $\int \int_0^{2\pi} G(t', t) dt' dt$ in terms of the Fourier coefficients as:

$$\begin{aligned}
\int \int_0^{2\pi} G(t', t) dt' dt &= 2\pi \int_0^{2\pi} F_{00} dp + 4\pi a_0 \int_0^{2\pi} F_{10} dp + 4\pi \sum_k |a_k|^2 \int_0^{2\pi} F_{20} dp + \\
&2\pi \sum_k |a_k|^2 \int_0^{2\pi} F_{21} e^{ir_0 k p} dp + 4\pi \sum_k |a_k|^2 i r_0 k \int_0^{2\pi} F_{23} e^{ir_0 k p} dp + \\
&2\pi \sum_k |a_k|^2 k^2 r_0^2 \int_0^{2\pi} F_{24} e^{ir_0 k p} dp \\
&= 2\pi \int_0^{2\pi} F_{00} dp + a_0 4\pi \int_0^{2\pi} F_{10} dp + \\
&\sum_k |a_k|^2 2\pi \left\{ \left[2 \int_0^{2\pi} F_{20} dp + \int_0^{2\pi} F_{21} e^{ir_0 k p} dp \right] + \right. \\
&k \left[2i r_0 k \int_0^{2\pi} F_{23} e^{ir_0 k p} dp \right] + k^2 \left[2\pi \int_0^{2\pi} F_{24} e^{ir_0 k p} dp \right] \left. \right\}. \quad (24)
\end{aligned}$$

Combining the length term (17), the area term (18), and the quadratic term (24), the active contour energy can be written as:

$$\begin{aligned}
E(\Gamma) &= \left[\lambda_C 2\pi r_0 + \alpha_C \pi r_0^2 - \frac{\beta_C}{2} 2\pi \int_0^{2\pi} F_{00} dp \right] \\
&+ a_0 \left[\lambda_C 2\pi + \alpha_C 2\pi r_0 - \frac{\beta_C}{2} 4\pi \int_0^{2\pi} F_{10} dp \right] \\
&+ \sum_k |a_k|^2 \left(\lambda_C \pi r_0 k^2 + \alpha_C \pi \right. \\
&- \frac{\beta_C}{2} 2\pi \left\{ \left[2 \int_0^{2\pi} F_{20} dp + \int_0^{2\pi} F_{21} e^{ir_0 k p} dp \right] \right. \\
&\left. \left. + k \left[2i r_0 \int_0^{2\pi} F_{23} e^{ir_0 k p} dp \right] + k^2 \left[r_0^2 \int_0^{2\pi} F_{24} e^{ir_0 k p} dp \right] \right\} \right). \quad (25)
\end{aligned}$$

B Other approaches for tree extraction

Here we review earlier publications on the subject. The first aerial image was acquired in Paris in 1856 by F. Tournachon. The image was taken from an air-balloon and the altitude was rather low. After 150 years, the fields have benefitted from space technology making use of modern satellite navigation technology (such as GPS) and high performance computers to improve their capabilities in many respects.

The problem of locating, counting or delineating individual trees in high resolution aerial images has been studied in several paper. Gougeon introduced a specialized knowledge about the object during segmentation (rule-based segmentation) [17] and presented a contour based feature extraction to utilize for delineation of single tree crowns, the contour is defined as a delimiter in the image, between the objects (tree crowns) and the background, a valley is a delimiter between two different image objects (valley following algorithm) [18]. Larsen introduced an algorithm based on template matching for Spruce top detection. He computed the model from the tree and its shadow, and reached good results with this method [26, 27].

Several contour based methods were defined for the problem of counting and locating trees. Brandtberg *et al.* presented a new approach. They extracted the contour and calculated the curvature over the contour. Then they matched circles to the contour with the aid of the curvature [5]. Bacher *et al.* introduced another contour-based method on very-high resolution aerial images, they extracted the skeleton of the trees during the spring [2]. Andersen *et al.* presented a morphological-based approach combined with a top-hat transformation for segmentation of individual trees [1]. Perrin *et al.* introduced a stochastic method with marked point process [36]. They define a disk model with variable radius and orientation. They use Reversible Jump Markov Chain Monte Carlo dynamics and a simulated annealing to get the maximum a posteriori estimator.

References

- [1] H.E. Andersen, S.E. Reutebuch, and G.F. Schreuder. Automated Individual Tree Measurement through Morphological Analysis of a LIDAR-based Canopy Surface Model. In *Proc. of the 1st International Precision Forestry Symposium*, pages 11–21, June 2001.
- [2] U. Bacher and H. Mayer. Automatic extraction of trees in urban areas from aerial imagery. *International Archives of Photogrammetry and Remote Sensing*, (33) B3/1, pages 51–57, 2000.
- [3] R. J. Baxter. *Exactly Solved Models in Statistical Mechanics*. Academic Press, 1990.
- [4] A. Blake and A. Zisserman. Visual reconstruction. *MIT Press, Cambridge - MA*, 1987.
- [5] T. Brandtberg and F. Walter. Automated delineation of individual tree crowns in high spatial resolution aerial images by multiple-scale analysis. *Machine Vision and Applications*, (11):64–73, 1998.
- [6] V. Caselles, F. Catte, T. Coll, and F. Dibos. A geometric model for active contours. *Numerische Mathematik*, 66:1–31, 1993.
- [7] V. Caselles, R. Kimmel, and G. Sapiro. Geodesic active contours. *International Journal of Computer Vision*, 22(1):61–79, 1997.
- [8] T. Chan and L. Vese. An Active Contour Model without Edges. In *SCALE-SPACE '99: Proceedings of the Second International Conference on Scale-Space Theories in Computer Vision*, pages 141–151. Springer-Verlag, 1999.
- [9] Y. Chen, H.D. Tagare, S. Thiruvenkadam, F. Huang, D. Wilson, K.S. Gopinath, R.W. Briggs, and E.A. Geiser. Using prior shapes in geometric active contours in a variational framework. *International Journal of Computer Vision*, 50(3):315–328, 2002.
- [10] Y. Chen, S. Thiruvenkadam, H. D. Tagare, F. Huang, D. Wilson, and E.A. Geiser. On the incorporation of shape priors into geometric active contours. In *Proc. IEEE Workshop VLISM*, pages 145–152, Vancouver, Canada, 2001.
- [11] L. D. Cohen. On active contours and balloons. *CVGIP: Image Understanding*, 53:211–218, 1991.

- [12] D. Cremers, C. Schnorr, and J. Weickert. Diffusion-snakes: combining statistical shape knowledge and image information in a variational framework. In *Proc. IEEE Workshop VLISM*, pages 137–144, Vancouver, Canada, 2001.
- [13] D. Cremers and S. Soatto. A Pseudo-distance for Shape Priors in Level Set Segmentation. In *2nd IEEE Intl. Workshop on VLISM*, Nice, France, Oct 2003.
- [14] D. Cremers, F. Tischhäuser, J. Weickert, and C. Schnörr. Diffusion Snakes: Introducing Statistical Shape Knowledge into the Mumford-Shah Functional. *International Journal of Computer Vision*, 50(3):295–313, 2002.
- [15] A. Foulonneau, P. Charbonnier, and F. Heitz. Geometric Shape Priors for Region-Based Active Contours. In *IEEE Conf. ICIP 2003, Barcelona, Spain*, Sept 2003.
- [16] S. Geman and D. Geman. Stochastic relaxation, Gibbs distributions and the Bayesian restoration of images. *IEEE Trans. Patt. Anal. Mach. Intell.*, 6:721–741, 1984.
- [17] F.A. Gougeon. A Crown-following Approach to the Automatic Delineation of Individual Tree Crowns in High Spatial Resolution Aerial Images. *Canadian Journal of Remote Sensing*, 21(3), pages 274–284, 1995.
- [18] F.A. Gougeon. Automatic Individual Tree Crown Delineation using a Valley-following Algorithm and Rule-based System. In D.A. Hill and D.G. Leckie, editors, *Proc. of the International Forum on Automated Interpretation of High Spatial Resolution Digital Imagery for Forestry*, pages 11–23, Victoria, British Columbia, Canada, Febr 1998.
- [19] U. Grenander. *General Pattern Theory*. Oxford University Press, Oxford, UK, 1993.
- [20] U. Grenander and M. Miller. Representations of knowledge in complex systems. *Journal of the Royal Statistical Society, series B*, 56:549–603, 1994.
- [21] R. Huang, V. Pavlovic, and D. N. Metaxas. A graphical model framework for coupling MRFs and deformable models. In *Proc. IEEE CVPR*, Washington, DC, USA, 2004.
- [22] S. Jehan-Besson, M. Barlaud, and G. Aubert. DREAM2S: Deformable regions driven by an Eulerian accurate minimization method for image and video segmentation. *International Journal of Computer Vision*, 53:45–70, 2003.
- [23] M. Kass, A. Witkin, and D. Terzopoulos. Snakes: Active Contour Models. *International Journal of Computer Vision*, 1(4):321–331, 1988.
- [24] Z. Kato, M. Berthod, and J. Zerubia. A hierarchical Markov random field model and multi-temperature annealing for parallel image classification. *Computer Vision, Graphics and Image Processing: Graphical Models and Image Processing*, 58(1):18–37, January 1996.
- [25] S. Kichenassamy, A. Kumar, P. Olver, A. Tannenbaum, and A. Yezzi. Gradient flows and geometric active contour models. In *Proc. ICCV*, Boston, MA, USA, 1995.
- [26] M. Larsen. Finding an optimal match window for Spruce top detection based on an optical tree model. In D.A. Hill and D.G. Leckie, editors, *Proc. of the International Forum on Automated Interpretation of High Spatial Resolution Digital Imagery for Forestry*, pages 55–66, Victoria, British Columbia, Canada, Feb. 1998.

- [27] M. Larsen. Individual Tree Top Position Estimation by Template Voting. In *Proc. of the Fourth International Airborne Remote Sensing Conference and Exhibition / 21st Canadian Symposium on Remote Sensing*, volume 2, pages 83–90, Ottawa, Ontario, June 1999.
- [28] M. E. Leventon, W. E. L. Grimson, and O. Faugeras. Statistical shape influence in geodesic active contours. In *Proc. IEEE CVPR*, volume 1, pages 316–322, Hilton Head, SC, USA, 2000.
- [29] R. Malladi, J. A. Sethian, and B. C. Vemuri. Shape modeling with front propagation: A level set approach. *IEEE Trans. Patt. Anal. Mach. Intell.*, 17:158–175, 1995.
- [30] D.N. Metaxas. *Physics-based Deformable Models: Applications to Computer Vision, Graphics and Medical Imaging*. Kluwer, 1997.
- [31] M. Miller and L. Younes. Group actions, homeomorphisms, and matching: A general framework. *International Journal of Computer Vision*, 41:61–84, 2002.
- [32] M. I. Miller, U. Grenander, J. A. O'Sullivan, and D. L. Snyder. Automatic target recognition organized via jump-diffusion algorithms. *IEEE Transactions on Image Processing*, 6(1):157–174, January 1997.
- [33] D. Mumford and J. Shah. Optimal Approximation by Piecewise Smooth Functions and Associated Variational Problems. *Comm. Pure Appl. Math.*, 1989.
- [34] S. Osher and J. A. Sethian. Fronts propagating with curvature dependent speed: Algorithms based on Hamilton-Jacobi formulations. *J. Comp. Phys.*, 79:12–49, 1988.
- [35] N. Paragios and R. Deriche. Geodesic active regions: A new framework to deal with frame partition problems in computer vision. *Journal of Visual Communication and Image Representation*, 13:249–268, 2002.
- [36] G. Perrin, X. Descombes, and J. Zerubia. Tree crown extraction using marked point processes. In *EUSIPCO, Vienna, Austria*, Sep. 2004.
- [37] M. Rochery, I. Jermyn, and J. Zerubia. Higher Order Active Contours and their Application to the Detection of Line Networks in Satellite Imagery. In *2nd IEEE Intl. Workshop on VLSM, Nice, France*, Oct 2003.
- [38] M. Rousson and N. Paragios. Shape priors for level set representations. In *Proc. ECCV, Lecture Notes in Computer Science*, pages 78–92, Copenhagen, Denmark, 2002. Springer.
- [39] J. A. Sethian. *Level Set Methods and Fast Marching Methods*. Cambridge Monograph on Applied and Computational Mathematics. Cambridge University Press, Cambridge, U.K., 2nd edition, 1999.
- [40] K. Siddiqi and B. B. Kimia. A shock grammar for recognition. In *CVPR '96, San Francisco, CA, USA*, pages 507–513, 1996.
- [41] R. Veltkamp and M. Hagedoorn. State-of-the-art in shape matching. Technical Report UU-CS-1999-27, Utrecht University, the Netherlands, 1999.